Sensors & Actuators: A. Physical 372 (2024) 115332

Contents lists available at ScienceDirect

Sensors and Actuators: A. Physical

journal homepage: www.journals.elsevier.com/sensors-and-actuators-a-physical

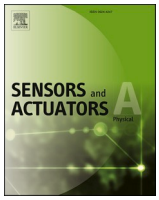

A tri-modal dielectric elastomer actuator integrating linear actuation, sound generation, and self-sensing capabilities

Sebastian Gratz-Kelly [a], Tim Felix Krüger [a], Stefan Seelecke [a], Gianluca Rizzello [a], Giacomo Moretti [b,*]

[a] Department of Systems Engineering, Saarland University, Saarbrücken 66123 Germany
[b] Department of Industrial Engineering, University of Trento, Trento 38123, Italy

ARTICLE INFO

Keywords:
dielectric elastomers
loudspeaker
tactile
self-sensing
user interfaces

ABSTRACT

This paper presents a concept of multi-modal dielectric elastomer actuator (DEA) that leverages a single voltage input to concurrently work as linear actuator and loudspeaker, while also integrating self-sensing capabilities. Low-frequency linear actuation is obtained by inducing tangential stretching of the DEA membrane surface, whereas high-frequency sound generation is concurrently achieved through transverse structural vibrations of the DEA membrane surface. Multi-mode actuation is combined with a new self-sensing paradigm: measuring the current signal arising from the dynamic acoustic excitation and processing it in real-time with capacitance estimation algorithms, the actuator low-frequency displacement can be reconstructed with no need for additional transducers or dedicated probing signals. The performance of the proposed self-sensing approach is evaluated using complex multi-harmonic driving signals, with a focus on analyzing the correlation between capacitance estimates and the low-frequency stroke of the device. Concurrent self-sensing and multi-mode actuation are finally demonstrated in a number of application scenarios, in which the intensity/frequency of the DEA acoustic output is adjusted in closed-loop as a function of externally induced deformations, such as impacts with obstacles, or interactions with a user. The multi-modality paradigm pursued in this work paves the way to new application opportunities, such as multi-sensory user interfaces (e.g. audio-tactile buttons), or highly integrated sensor-actuator units able to sense their state during operation and provide feedback (e.g., acoustic signaling) accordingly.

1. Introduction

Dielectric elastomers (DEs) are a promising actuator and sensor technology for mobile devices, wearables, and interaction interfaces, because of their high stretchability, low weight, ability to accomplish self-sensing [1]. DE transducers rely on a variable capacitance principle enabled by stretchable polymeric membranes coated by compliant electrodes, which can be deformed through the application of an electric field [2,3]. Available DE materials include acrylics, rubber, or silicone, which can provide electrostatic actuation stresses on the order of MPa, and strains over 100 % [4,5]. DEs lend themselves to integration onto soft-robotic structures (e.g., minimum energy-structures [6]) and metamaterials [7], and their actuation capability spans broad bandwidths from less than 1 Hz up to several kHz [8,9].

A special field of interest for DEs is represented by user interfaces and wearables [10–15]. In this context, the possibility of embedding different actuation functionalities (e.g., vibrotactile actuation, sound generation) within a single multi-functional DE actuator (DEA) unit might provide a breakthrough in user interaction applications [16]. In a previous work, we showed that with certain DEA topologies, low frequency (LF) linear actuation (associated to a longitudinal stretching of a DE membrane) and high frequency (HF) structural vibrations can be induced simultaneously and independently by a single input voltage, hence allowing a DEA device to work as LF linear actuator and loudspeaker, in a multi-modal fashion [16,17].

A different paradigm of multi-modality that has largely been exploited in the past on DEAs is self-sensing, i.e., the possibility of using a transducer as an actuator and a sensor at the same time. Self-sensing

Abbreviations: CC, Correlation coefficient; COP, Circular out-of-plane; DE, Dielectric elastomer; DEA, Dielectric elastomer actuator; HF, High frequency; LF, Low frequency; MF, Mid frequency; NBS, Nonlinear biasing spring; PLA, Polyactic acid; RC, Resistor-capacitor circuit; SPL, Sound pressure level.

* Corresponding author.
E-mail address: giacomo.moretti@unitn.it (G. Moretti).

https://doi.org/10.1016/j.sna.2024.115332
Received 13 February 2024; Received in revised form 1 April 2024; Accepted 2 April 2024
Available online 6 April 2024

enables closed-loop control to be implemented in DEAs without the need for additional mechanical sensors [18]. Self-sensing algorithms usually reconstruct the DEA capacitance, and, in turn, its mechanical deformation, by online processing electrical measurements (i.e., voltage and current) acquired during high voltage actuation [19–23]. Due to the capacitive nature of DEAs, the current generated by typical LF actuation (on the order of a few Hz) is generally too small to be accurately measured and integrated, thus compromising the accuracy of self-sensing. To overcome this issue, DE self-sensing algorithms commonly rely on the injection of a small-amplitude HF monochromatic sensing signal (purposedly introduced for the aim of sensing) on top of the main driving signal, which generates a high-amplitude current without affecting the actuator mechanical response [22,23].

Combining multi-frequency actuation with self-sensing might deliver radically new applications, such as wearable multi-function devices (e.g. audio-tactile interfaces) that might help improving human-machine interaction in industry by adding intuitive input and feedback elements to control machines, or highly integrated wearable feedback interfaces for virtual reality.

Motivated by these applications, the present work demonstrates the first example of tri-modal DEA, in which three independent functionalities (i.e., LF linear actuation, HF sound generation, and self-sensing) are integrated into a same active DE element and executed simultaneously. First, we show a characterization of the frequency response of a reference DEA design in terms of sound pressure and deformation. We then consider a self-sensing algorithm from literature [22], originally built upon the assumption of sinusoidal HF probing signal. Due to its time-domain (rather than frequency-domain) nature, the algorithm can effectively capture capacitance variations in real time even when polychromatic HF input signals are used. Leveraging the DEA dynamic response, we use different regions of the frequency response to perform self-sensing while either enforcing sound generation (using a single driving signal for sensing and sound generation) or preventing it (by performing sensing through the injection of mid-frequency signals that fall outside of the acoustic bandwidth of the device).

To prove the real-time capability of the proposed multi-modal paradigm, we present several proof-of-concept examples, which are representative of possible applications, including HF amplitude or frequency adaption driven by externally-induced sensed deformations, application of the DEA as a smart button capable of deformation-dependent audio-tactile feedback, and acoustic signaling upon impact detection.

To the best of our knowledge, this is the first work that combines multi-modal DE actuation with self-sensing in closed loop operations. Compared to our preliminary findings on self-sensing with multi-chromatic signals [24], here we present for the first time a systematic analysis of the accuracy and performance of self-sensing in combination with multi-mode actuation, and we demonstrate its applicability in real-time scenarios.

The remainder of this paper is structured as follows. Section 2 describes the layout and working principle of the multi-mode DEA. Section 3 describes the proposed self-sensing approach and its synergies with the multi-mode actuation principle. Section 4 shows the results of characterization measurements aimed at evaluating the self-sensing algorithm's capability and accuracy. Section 5 describes proof-of-concept demonstrations and results. Section 6 presents the conclusion and outlook for future developments.

2. DEA layout and working principle

The considered DE topology is a circular out-of-plane DEA (COP-DEA), devised to provide linear actuation [25,26]. The DEA element consists of a stack of DE membranes, each one having a single electrode layer on one face (Fig. 1). Consecutive electrodes are subjected to opposite voltage polarities, so that the resulting DE stack forms a capacitor with 4 parallel dielectric layers and a passive external coating layer. The stack, initially flat, is radially pre-stretched on a rigid annular frame, and is pre-loaded out of plane by a nonlinear biasing spring (NBS).

When a LF input voltage is applied, the device end-effector (consisting in a rigid disc concentric to the DEA electrodes) moves out of plane and delivers a stroke z in the axial direction (Fig. 1). This out-of-plane motion is a consequence of the membrane longitudinal stretching generated by the electrostatic pressure (Maxwell pressure), which is proportional to the square of the applied voltage. When a HF voltage waveform (with frequency higher than the out-of-plane mode's natural frequency) is applied, the out-of-plane displacement progressively decreases as a result of the low-pass behavior of the end-effector dynamics, and the membrane surface develops a set of structural vibration modes similar to the ones observed in flat circular/annular vibrating membranes [27]. In previous works [16,17] we observed that, for COP-DEAs with radial dimensions in the centimeter range, an acoustic response (hearable sound pressure output) is generated in the working ranges where HF structural vibrations take place, triggered by excitation

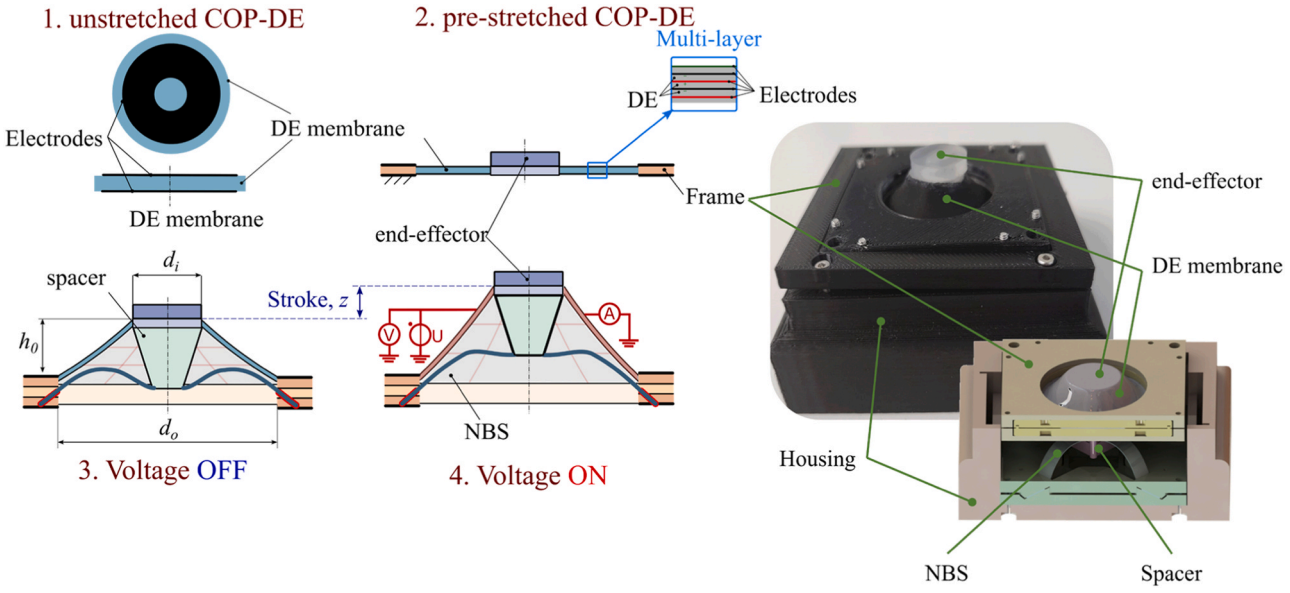

Fig. 1. COP-DEA structure, with pre-stretching element (NBS) and layered membrane. Picture and 3D model of the DEA element under investigation.

voltages with relatively small amplitudes on the order of hundreds of volts. Due to the significant difference in the end-effector and the DE membrane inertia, structural vibrations of the DEA surface and linear stroke are generated on clearly separated regions of the frequency domain. Therefore, a simultaneous and independent activation of linear actuation and sound generation mode is possible by driving the actuator with a voltage input which is the sum of two terms:

$$v(t) = \sqrt{V_0 + V_1\overline{u}(t)} + U_a\widetilde{u}(t), \text{ with}$$
$$V_0 = \frac{U_{max}^2 + U_{min}^2}{2},\ V_1 = \frac{U_{max}^2 - U_{min}^2}{2} \quad (1)$$

The first term in (1), i.e., the one under square root, represents a high-amplitude driving signal with LF fundamental frequency, whereas the second term is a HF low-amplitude signal. In the equation, $\overline{u}(t)$ and $\widetilde{u}(t)$ are normalized waveforms (varying between -1 and $+1$) whose spectral content/fundamental components lie in a LF and a HF region respectively; U_{max} and U_{min} are the maximum/minimum voltage applied on the DEA when no HF component is present ($\widetilde{u} = 0$); U_a is the amplitude of the HF excitation component (we assume $U_a \ll U_{min}$). The square root in the first term is introduced to compensate for the nonlinear (i.e., quadratic) dependence of the electrostatic stresses (Maxwell stress) on v.

We manufactured a COP-DEA sample (Fig. 1, right) with outer diameter $d_o = 30$mm and inner diameter $d_i = 15$ mm. The material used for the dielectric layers is silicone Elastosil 2030 film by Wacker, with initial thickness of 50 μm. The DEA sample consists of 4 active layers (with both faces covered by compliant electrodes) and one passive layer (holding no electrode on one of its faces), which are stacked together. Electrodes were applied to the pre-stretched silicone films (equi-biaxial pre-strain of 20 %) in the desired geometry with a thickness on the order of 10 μm, via the screen printing process described in [28,29]. The electrode material is a composite of PDMS (SilGel 612 by Wacker) and carbon-black particles (Orion Printex XE2). The electrical connections to the electrodes were done with thin self-gluing copper foils. The NBS consists of two overlapped 50 μm thick spring steal foils and has the dimensions discussed in [16]. The NBS holder and the housing structure for the DEA are 3D printed with photopolymers and PLA. The initial out-of-plane deformation of the DEA is approximately 5 mm.

3. Self-sensing approach

In this section, we present a self-sensing approach and algorithm for multi-mode DEAs. The proposed approach leverages different regions of the DEA frequency response to accomplish deformation sensing either in combination with sound generation or alone in a silent mode. The sensing algorithm used here makes use of our previous results on self-sensing [18], obtained with monochromatic probing signals, which are here extended to multichromatic driving voltages.

3.1. Combined multi-mode self-sensing concept

In previous works [17], combined LF actuation and HF sound generation have been used to develop audio-tactile interfaces capable to provide multiple feedbacks (linear actuation, sound) through a single active DE element. An additional functionality can be added on top of such multi-mode actuation capability by means of self-sensing.

Self-sensing relies on voltage and current measurements on the DE to provide a real-time estimation of the DEA capacitance, which can be used to reconstruct the device stroke/configuration during high voltage actuation. Self-sensing is typically achieved by superposing a dedicated small-amplitude HF signal on top of the main (typically LF) driving voltage signal. Injected signals with sufficiently high frequency generate sufficiently large current outputs, which can be accurately measured and used in self-sensing algorithms [21].

Here, we propose an alternative self-sensing approaches that specifically leverage the COP-DEA dynamic response, and especially the HF excitation components present in multi-mode and audio-tactile DEA applications. On the one hand, when the device operates in the HF region producing an acoustic output, current measurements associated to the HF actuation signal component can be directly used for self-sensing without adding extra hardware (e.g., dedicated capacitive sensing layers, as proposed in [17]) or dedicated superposed sensing signals (because the current resulting from acoustic actuation is already large enough to be accurately measured). On the other hand, if no acoustic output is requested, self-sensing can still be performed by injecting a dedicated small-amplitude sensing signal (superposed to the LF driving signal, if present) with spectral content in an intermediate mid-frequency (MF) region where neither linear actuation or acoustic output are produced (Fig. 2). In this case, the driving voltage still has the form given by Eq. (2) (with $\widetilde{u}$ representing the MF sensing signal), but the choice of the sensing signal $\widetilde{u}$ frequency deliberately prevents (or strongly limits) sound generation.

Self-sensing in either of the two regions (MF or HF) can be further associated to different application scenarios, as shown in Fig. 3. In a first set of applications, the multi-mode DEA can be used with a HF/MF signal superimposed to a LF voltage signal to produce a voltage-induced displacement (left-hand side Fig. 3). The self-induced capacitance change of the DEA can then be estimated by a self-sensing algorithm and used to compute the motion of the end-effector. By feeding the DEA with a HF or a MF signal, self-sensing is thus accomplished either in combination with sound generation or alone. In a second scenario (right-hand side Fig. 3), the device deformation can be induced by an external mechanical stimulus. This scenario is representative of applications such as multi-mode audio-tactile buttons. In this case, the device deformation (measured via self-sensing) is driven by a user's touch, and can be accompanied by a vibrotactile stimulation via LF driving and/or sound through a HF superposed voltage signal. Also in this scenario, a silent self-sensing mode (for the external deformation) were no sound is produced can be realized leveraging the MF range rather than the HF range. Measuring the capacitance potentially allows generating adjustable multi-mode outputs (e.g., audio-tactile feedbacks) that are functions of the measured user input (e.g., touch).

3.2. Self-sensing algorithm

With the aim of formulating a self-sensing algorithm, we model the DEA electrical dynamics with an RC series circuit accounting for the DEA capacitance and electrodes resistance, while we neglect the leakage resistance, assuming that it is very high [21]. Though such an RC-series model represents a rough approximation of the DEA electrical response,

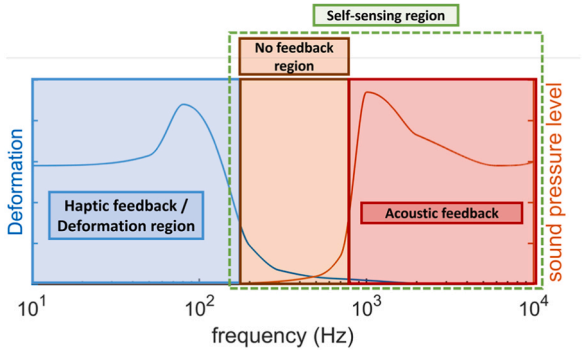

Fig. 2. Working regions of the multi-mode DEA, namely, LF linear motion region, MF region (with no acoustic output), and HF acoustic output region. Self-sensing can be performed leveraging voltage components in the MF and HF regions (and possibly part of the LF region). The plot is qualitative: frequency ranges shown on the frequency axis are an approximate indication that holds true for centimeter-scale DEAs with features/material properties similar to those discussed in [16,17] and in the present work.

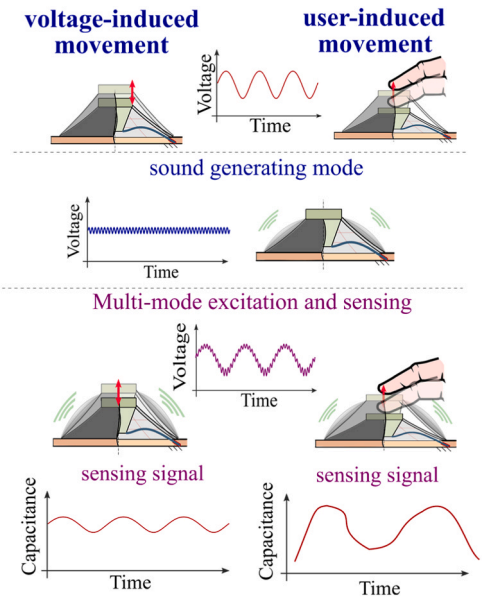

Fig. 3. Different working scenarios for the COP-DEA. Left: multi-mode actuation with HF structural vibrations and LF linear actuation, combined with two alternative modes for self-sensing (HF acoustic working mode and MF silent working mode). Right: operation as smart button, with user-driven LF deformation combined with two possible self-sensing modes (HF working mode with sound generation, and MF silent working mode).

we found that it accurately captures the relevant dynamics in the frequency ranges that are relevant to our application (see Supplementary Material, Sect. S3).

The equivalent RC circuit is described by the following dynamic equation:

$$v(t) = R(t)i(t) + \frac{1}{C(t)}\int_0^t i(\tau)d\tau \tag{2}$$

where the driving voltage signal $v(t)$ includes a HF component $\tilde{u}$ with much higher frequency than the longitudinal deformation frequency of the DE (see Eq. (1)), which in turn leads to high amplitude HF current $i(t)$. The DEA capacitance $C(t)$ and series resistance $R(t)$ are assumed to vary slowly due to LF excitation (i.e., an externally applied deformation, or a LF driving voltage component $\bar{u}$), whereas capacitance/resistance variations due to $\tilde{u}$ are assumed negligible (as they lead to small-amplitude structural vibrations). With this assumption, the resistance and the capacitance can be considered constant on time scales on the order of the HF excitation periods, whereas the time derivatives of $v(t)$ and $i(t)$ are dominated by HF components.

To estimate the slowly-varying parameters $C(t)$ and $R(t)$, DE self-sensing approaches commonly rely on a frequency domain approach [23]. In this case, the DE capacitance and electrode resistance are obtained in real time as a function of the amplitude change and phase shift between voltage and current. Since this approach relies on an electrical impedance argument, it requires the injected HF signal to be sinusoidal, a condition that does not hold true if a polychromatic HF signal (such as an acoustic waveform) is used. To ensure self-sensing in the presence of polychromatic HF signals, the self-sensing approach developed by Rizzello et al. [21,22] is used in this work. Being based on a time-domain (rather than frequency-domain) identification approach, this self-sensing strategy is virtually transparent to the waveform of the excitation signal. As the method is based on a discrete-time identification algorithm, Eq. (2) is discretised using the pre-warped Tustin method, obtaining:

$$v_k - v_{k-1} = R(i_k - i_{k-1}) + \frac{K_T}{C}(i_k + i_{k-1}) \quad \text{with}$$
$$K_T = \frac{\sin(\pi f_e T_s)}{2\pi f_e T_s} \tag{3}$$

where k represents a discrete time index, K_T is the pre-warp coefficient for Tustin method, with f_e representing the frequency of $\tilde{u}$ (if monochromatic) and T_s the sampling time step [22]. Estimation of the DEA capacitance C and resistance R at time instant k is performed based on voltage and current values measured at time instants k and $k-1$, by solving in real-time the linear regression problem (3) with a recursive least-squares method. A forgetting factor is also employed to account for slow variations in C and R [21].

The pre-warped Tustin method is introduced to counteract non-linear frequency warping effects due to time discretization. Compared to other discretization schemes (e.g., Euler method), pre-warped Tustin provides an accurate estimation of R and C even when the HF signal is sampled with a low resolution. In principle, the employed discretization method provides a theoretical estimation accuracy of 100 % only if a sinusoidal HF signal at frequency f_e is used. Nevertheless, the discretization given by Eq. (3) is still expected to approximate its continuous-time counterpart (2) with sufficient accuracy even in case of polychromatic HF signals, provided that their spectral content is concentrated around f_e. In this work, we prove that the estimation accuracy is still satisfactory even when the concentration of the HF signal spectrum around f_e is relatively broad.

4. Characterization of multi-mode DEA self-sensing

In this section, we present a characterization of the self-sensing behavior of the COP-DEA in combination with multi-mode operation. First, we investigate the frequency-dependent performance of the device in terms of linear actuation (LF working regions) and sound generation (HF working regions), and we identify suitable MF regions for pure self-sensing. Afterwards, we present an evaluation of the self-sensing algorithm for the cases of externally-driven and voltage-induced deformations, using sinusoidal and multichromatic (soundtrack) HF signals for concurrent sound generation and self-sensing. Eventually, a parametric study of the correlation among linear stroke and capacitance profiles estimated via self-sensing is presented.

4.1. Experimental setup

For the characterization measurements, a dedicated test setup was used (Fig. 4). The test setup consists of a data acquisition system with analog inputs/ outputs, a custom built sound-absorbing box (110 cm × 100 cm × 80 cm, as described in [16]), a microphone for acoustic measurements (Microtech Gefell MM210 with M33 conditioning module), a laser to measure the end-effector displacement (optoNCDT from micro epsilon), and a linear motor (Aerotech ANT-25LA) to drive the movement of the DEA end-effector. The microphone was located at a distance of 0.35 m from the sample and placed at a small angle (<20°) with respect to the axis of the DE device to prevent a shielding effect from the laser sensor, which was centrally aligned with the end-effector. In a previous work [17], we showed that the SPL response of the COP-DEA is nearly independent of the angle in an interval [-30°, +30°]. A high voltage amplifier (HA51U–3P5 by hivolt.de Gmbh & Co.KG with 3000 V maximum voltage and 10 mA maximum current), installed outside of the acoustic box, was connected to the DE. The amplifier has built-in voltage monitor used to measure the output voltage. The current through the DEA was measured with a custom current sensor.

The datasets presented in the following were acquired using the analog input and output channel of a PSV-500 3D laser vibrometer by Polytec at a sample rate of 50 kHz. The acoustic signals were pre-processed by a Matlab script to eliminate LF disturbances via a Fast-

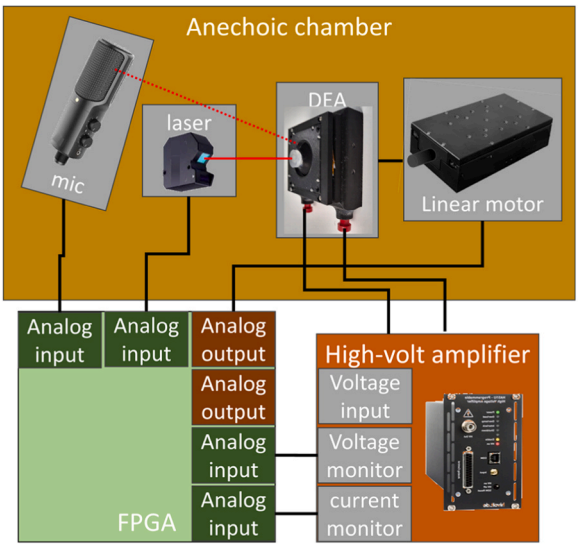

Fig. 4. Test rig setup for characterization measurements of the self-sensing performance of the multi-mode DEA.

Fourier Transform decomposition and reconstruction.

4.2. Frequency response and self-sensing algorithm characterization

We hereby characterize the COP-DEA prototype stroke and acoustic output frequency response, to identify the different frequency regions of the device (LF, MF and HF), and we present results from multi-mode self-sensing.

Fig. 5 shows the frequency response of the COP-DEA prototype in terms of deformation and SPL, obtained by exciting the DEA with chirp signals with different bias voltages ($U_{\max} = U_{\min}$ in Eq. (1), with $\widetilde{u}$ representing a unit amplitude chirp) and amplitudes (U_a). Chirp signals with a frequency range of 40–400 Hz and 1 – 3000 Hz were used for the deformation response and the acoustic response respectively.

In the region between 150 Hz and 600 Hz, the deformation and the sound pressure generated by the unit are very low. With that observation, the MF and HF regions for the self-sensing can be identified as 150–600 Hz and > 600 Hz, respectively. In the HF region, the unit produces sound with SPL of up to 90 dB.

We characterized the performance of the self-sensing algorithm in both scenarios illustrated in Fig. 3, with deformations induced by an external force (obtained via a linear motor connected to the COP-DEA end-effector), or by the LF components of the excitation voltage.

Fig. 6 shows a characterization of the unit performance and self-sensing capability in the presence of an external deformation input applied by a motor. The unit is driven with a HF signal $\widetilde{u}$ (either a sinusoidal signal with frequency of 700 Hz or a polychromatic audio track) used to produce an audible sound as well as to perform self-sensing. The audio track used for the tests presented here is the *Pokémon Center* jingle (transcribed by Project Nayuki [30]), whose spectrometer is reported in the supplementary materials. For both cases, a deformation with amplitude of 2 mm and frequency of 1 Hz is applied by the motor, and the acoustic output is measured with a microphone. The voltage input has a maximum amplitude of 200 V, bias of 2 kV, and produces maximum sound pressure on the order of 0.15 Pa (74 dB). The test with monochromatic excitation shows that the sound pressure amplitude changes as a function of the stroke (reaching a maximum when the COP-DEA out-of-plane deformation is maximum). This beating distortion, already observed in [16], is due to the nonlinear dynamics of the system, whose stiffness (in the structural HF modes) depends on z.

Correlation between the measured end-effector stroke and the sensed capacitance is quantified in terms of Pearson correlation coefficient (CC) between displacement and capacitance time signals. Such quantity is defined as the ratio between the covariance of the two variables and the product of their standard deviations, and is computed via the Matlab function *corrcoef*. The Pearson CC measures the linear correlation of the two variables with a result between −1 and 1 (+/- 1 perfect correlation; 0 no correlation) [31].

The CC between the calculated capacitance and the movement of the end-effector is 0.99 in the case of sinusoidal driving signals, and 0.83 in the case of polychromatic driving signals. The high level of correlation is confirmed by capacitance-stroke plots in Fig. 6 (bottom), which show that the two measured signals are related by a monotonic functional relationship. A comparison of the capacitance calculated by the self-sensing algorithm and a geometric model of the COP-DEA (derived in [26] and reported in the supplementary material) shows also that the signal shape is consistent with theoretical predictions. The variation of

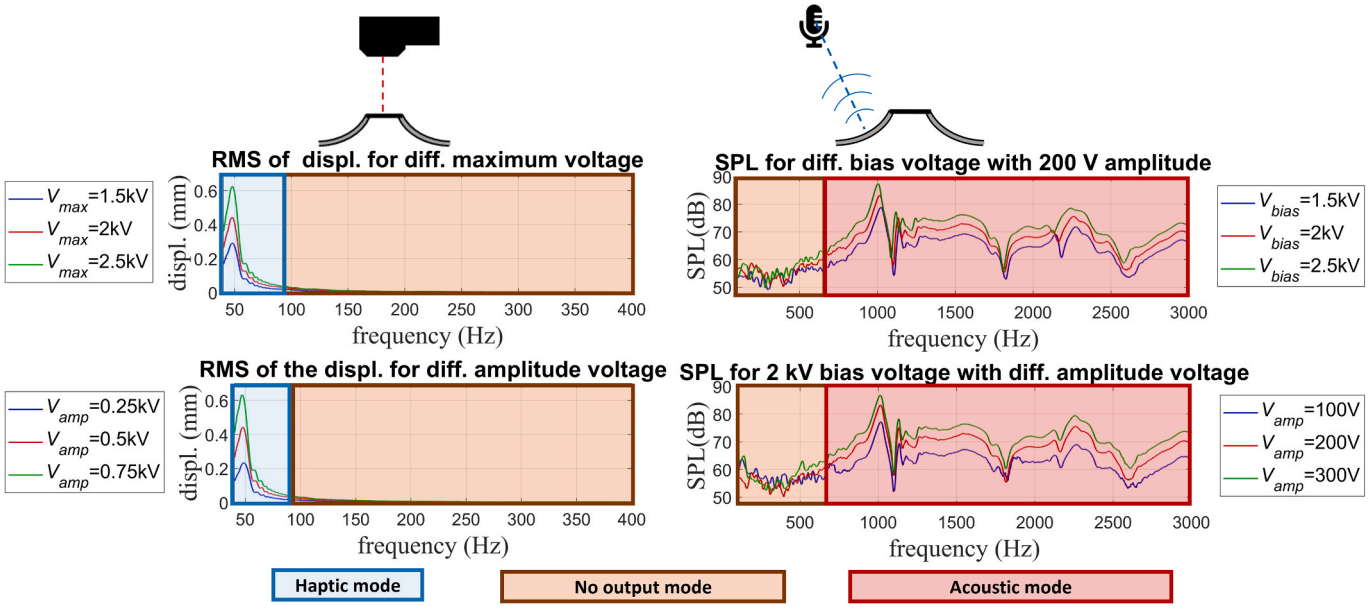

Fig. 5. COP-DEA frequency response in terms of displacement and sound pressure output, highlighting the LF (linear actuation mode), MF (no acoustic output mode) and HF regions (acoustic output mode) of the response.

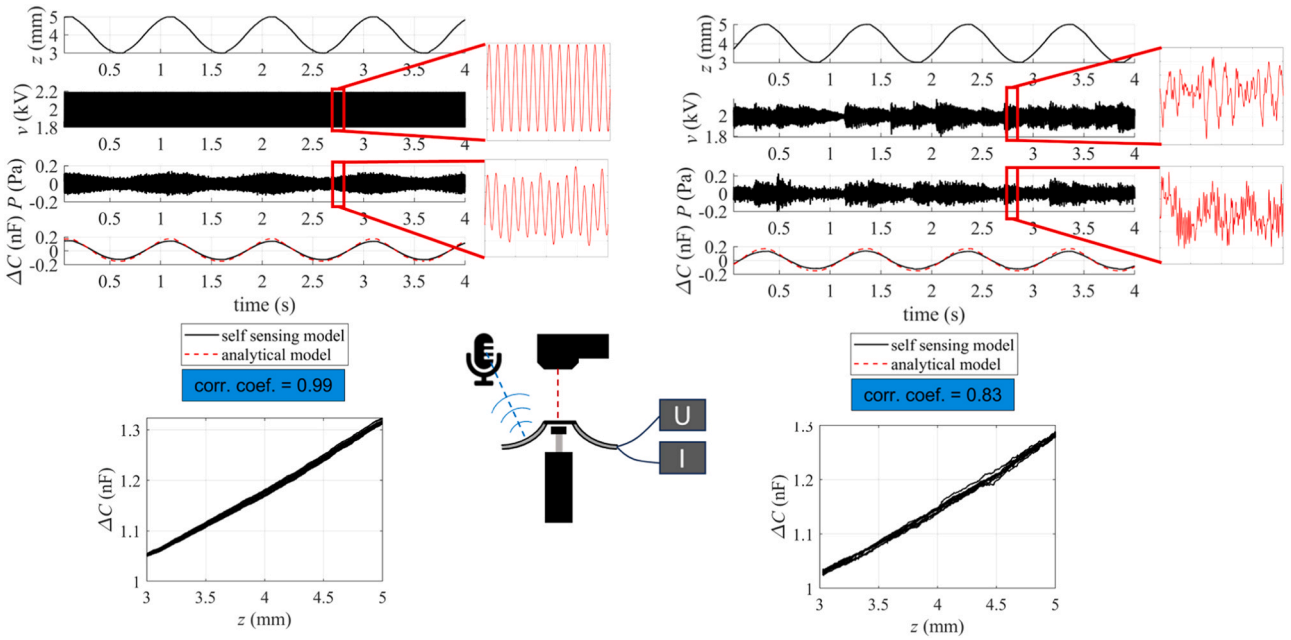

Fig. 6. Self-sensing performance for motor-induced movement Left: sinusoidal HF signal $\tilde{u}$ (700 Hz). Right: HF signal $\tilde{u}$ rendering a soundtrack.

the capacitance ΔC is calculated by subtracting the initial (equilibrium) value of the measured capacitance (which includes parasitic effects due to electrode portions that lie outside of the useful actuator area, underneath the rigid frames, difficult to include in the model).

In a similar fashion, self-sensing in the presence of a voltage-induced deformation of the DEA element is characterized in Fig. 7. In this case, a LF signal with $U_{\min} = 500$ V and $U_{\max} = 2500$ V is superimposed to a HF signal with same amplitude and frequency as in the previous motor-induced measurements. The deformation of the end-effector is below 0.5 mm, and the maximum sound pressure is on the same order as for motor-induced measurements. Compared to the previous case, fluctuations in sound pressure amplitude are much higher. This can be explained by changes in bias voltage due to the LF signal. The bias voltage has an even higher influence than the out-of-plane deformation on the stiffness associated the structural modes: increasing the voltage leads to a reduction in the DE membrane stiffness, which in turn leads to larger amplitude vibrations and sound pressure output.

The CC for the sinusoidal HF signal (0.87) is lower than that measured in the case of motor induced displacement. This is due to a ripple in the trend of the estimated capacitance, occurring in the low voltage range. This peak is an artifact possibly due to multiple concurrent causes: 1) in addition to out-of-plane conical deformations, electric activation causes a static lateral deformation of the COP-DEA against the membrane profile necking, which leads to a change in capacitance; 2) the power supply output is subject to distortions in the considered frequency range, due to dynamic effects and the capacitive load created by the DEA. Both above mentioned effects become particularly conspicuous when end-effector displacements are small, as in the example considered

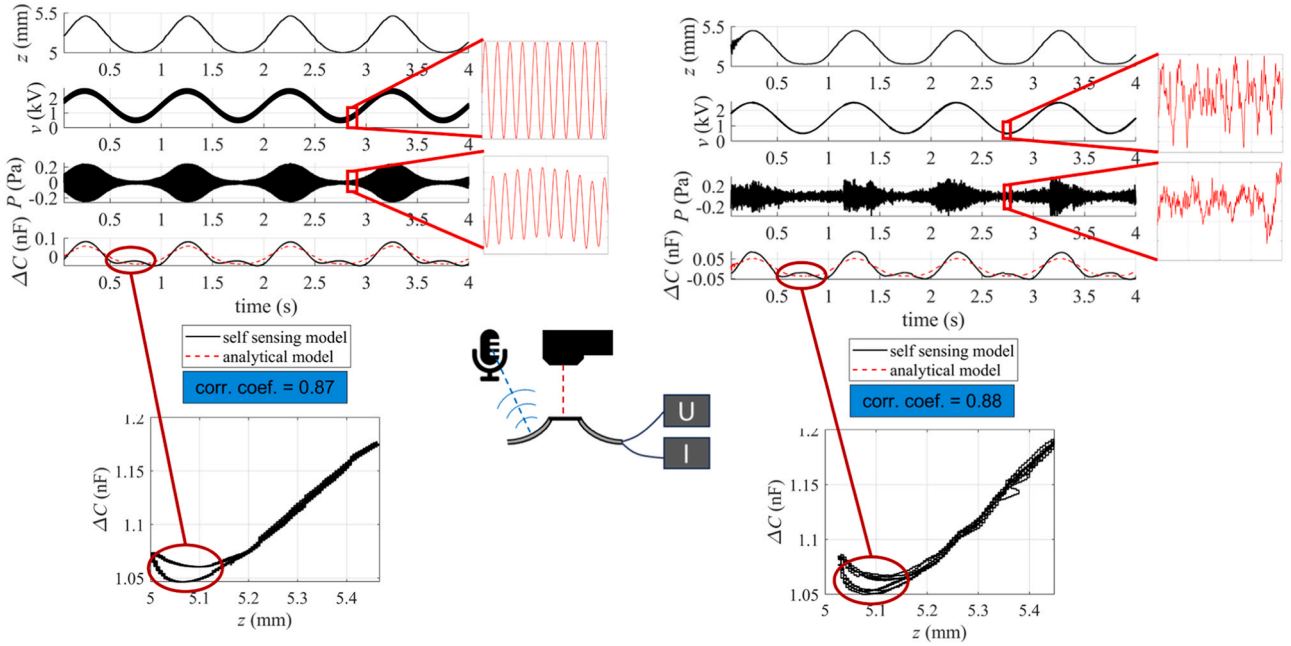

Fig. 7. Self-sensing performance for voltage-induced movement Left: sinusoidal HF signal $\tilde{u}$ (700 Hz). Right: HF signal $\tilde{u}$ rendering a soundtrack.

here. The mismatch between actual displacement and estimated capacitance in the bottom part of the stroke is also reflected in the capacitance-displacement trend, shown in Fig. 7 (bottom) for 4 cycles. Whereas the trend shows a monotonic functional behavior over a large portion of the stroke range (similar to Fig. 6), the univocal correlation between displacement and predicted capacitance is not correctly estimated in the bottom part of the stroke ($z \in [5.0, 5.2]$ mm).

Despite such misestimation of the capacitance over restricted portions of the stroke range, the global CC is higher than 0.8, and the algorithm is able to macroscopically capture the trend of z. In the case of measurements performed using a song as the HF signal, the CC (0.87) is the same as for sinusoidal HF signals. Comparison of the capacitance trends estimated via self-sensing and with the geometrical model (based on measurements of z) shows a greater deviation compared to that observed in tests with motor-driven deformation (Fig. 6). This happens because, in this test, capacitance varies in a narrower range, leading to higher relative inaccuracy in the capacitance estimate.

Results show that the self-sensing algorithm based on HF driving signals (either monochromatic or broadband) in the acoustic range leads to capacitance estimates that accurately replicate the essential features of the DEA linear displacement. With this consideration, it is also possible to use arbitrarily complex polychromatic signals (soundtracks) to produce an acoustic output while simultaneously performing sensing.

4.3. Parametric characterization study

In this section, we present the results of an extended set of measurements, performed with the same procedure as in Fig. 6 and Fig. 7, by varying a broad set of test parameters with the aim to evaluate the robustness of the self-sensing algorithm.

For motor-induced measurements, we performed tests at different frequencies and amplitude of the HF driving signal as well as different biasing voltages, while prescribing LF sinusoidal deformations with different frequencies (1 Hz and 3 Hz) and amplitudes.

Tests with different frequencies of signal $\widetilde{u}$ were executed using an amplitude $U_a = 200$ V and biasing voltage $U_b = 2$ kV, with displacement of 2 mm amplitude and 1 Hz frequency performed by the linear motor. Tests with different values of amplitude U_a were carried out at constant biasing voltage of 2 kV, and same LF deformations as in the previous case. Tests with different bias voltages were run using a HF amplitude of 50 V (which allowed us to apply different bias voltages, including low bias voltages, while preserving the voltage polarity positive) and same LF deformations as before. Tests with different prescribed deformation amplitude were done using a HF signal of 200 V amplitude, 350 Hz frequency, and 2 kV bias voltage.

Results are summarized in Fig. 8 in terms of SPL and CC between estimated capacitance and measured displacement. The points for the SPL in the plot in Fig. 8 are the mean values of the SPL over the complete time window of the measurement. The CC is over 0.9 for all parameter combinations, and it decreases below 0.9 only for very low frequencies below 50 Hz.

In the considered region (below the natural frequency of the first structural mode), the SPL increases with increasing frequency, and depends on the HF amplitude and the bias voltage as previously observed. Lowest SPL values reported in these tests corresponds to a condition in which the DEA produces no sound, despite minimum values displayed in the plots are on the order of 40–50 dB, because of limitations in the microphone and electronics capability.

The results provide evidence that, in all configurations, it is possible to identify regions where high SPL can be generated while concurrently obtaining capacitance measurements with CC close to 1, or regions where the CC is still high but no sound is produced. This allows implementing scenarios where sensing is accomplished either in combination with or independently of sound generation.

We repeated the characterization using a soundtrack (spectrometer in supplementary material) as HF signal. Corresponding results are shown in Fig. 9. In this case, the obtained CC is sensibly lower. The bias voltage and the amount of mechanical deformation have the most significant influence on the CC, whereas amplitude U_a has a minor influence on the CC. For bias voltages higher than 1.5 kV and displacements over 2 mm, the CC is higher than 0.8. It can be concluded that also with a polychromatic signal the self-sensing algorithm is able to provide capacitance estimates that are highly correlated with the device stroke, for a broad range of different parameters of the driving acoustic signal.

We characterized the parametric response of the system in the presence of LF voltage-driven deformations and a superposed HF excitation. Results obtained with a monochromatic sinusoidal HF signal are shown in Fig. 10(a). In a first set of tests (Fig. 10(a) top), a monochromatic HF excitation component with amplitude of 200 V and different frequencies was applied. Another set of tests (Fig. 10(a) center) was performed using a HF signal with 1 kHz frequency and different amplitudes. In both cases, the voltage of the LF driving signal is chosen as a 1 Hz sine wave varying within the range 0.5–2.5 kV. In a last set of tests (Fig. 10(a) bottom), a constant HF signal component (1 kHz, 200 V) was used, and the frequency and amplitude of the LF component were changed. The LF signal bias was chosen in such a way that the voltage waveform had minima at 500 V.

In addition to SPL and CC, we isolated and quantified the contribution of the HF signal to the end-effector displacement (magenta x-markers). This was done by applying a low-pass filter to the displacement measurement and subtracting the LF position signal (green circular markers) from the initial signal. The values for the HF displacement values were then calculated by using the average of the envelope of the resulting signal (using the envelope function in Matlab). Tests with variable HF signal amplitude and LF amplitude were also performed using a soundtrack as the HF signal (Fig. 10(b)).

The contribution of the HF signal $\widetilde{u}$ to the stroke is generally small (on the order of micrometers), because of the high frequencies and small

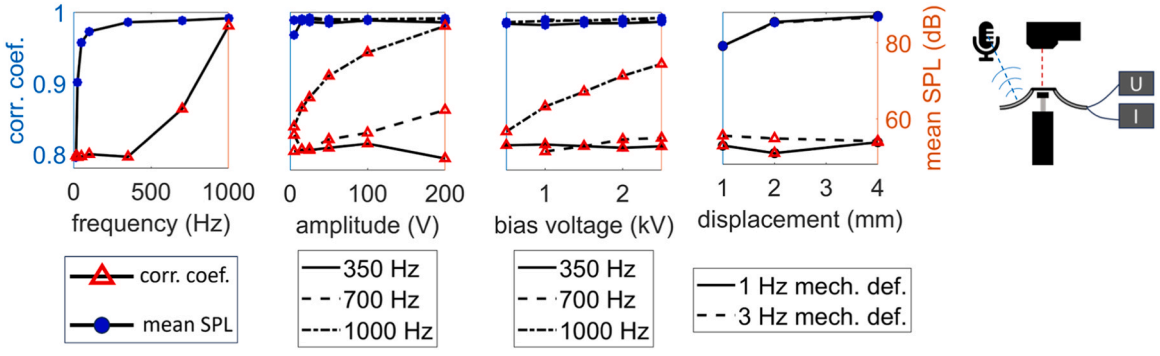

Fig. 8. Characterization of CC based on self-sensing (dot markers) and SPL (triangular markers) for different parameter choices, with motor-induced movement and sinusoidal HF excitation.

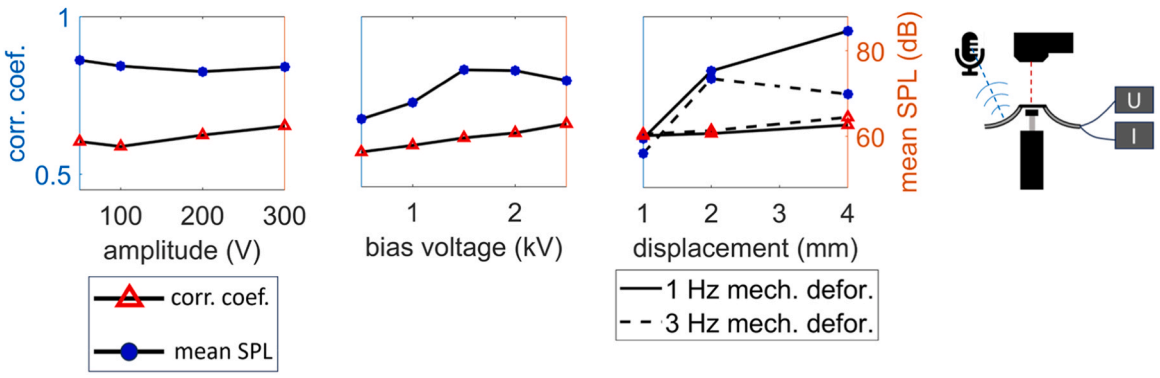

Fig. 9. Characterization of CC based on self-sensing (dot markers) and SPL (triangular markers) for different parameter choices, with motor-induced movement and polychromatic HF signal (soundtrack.

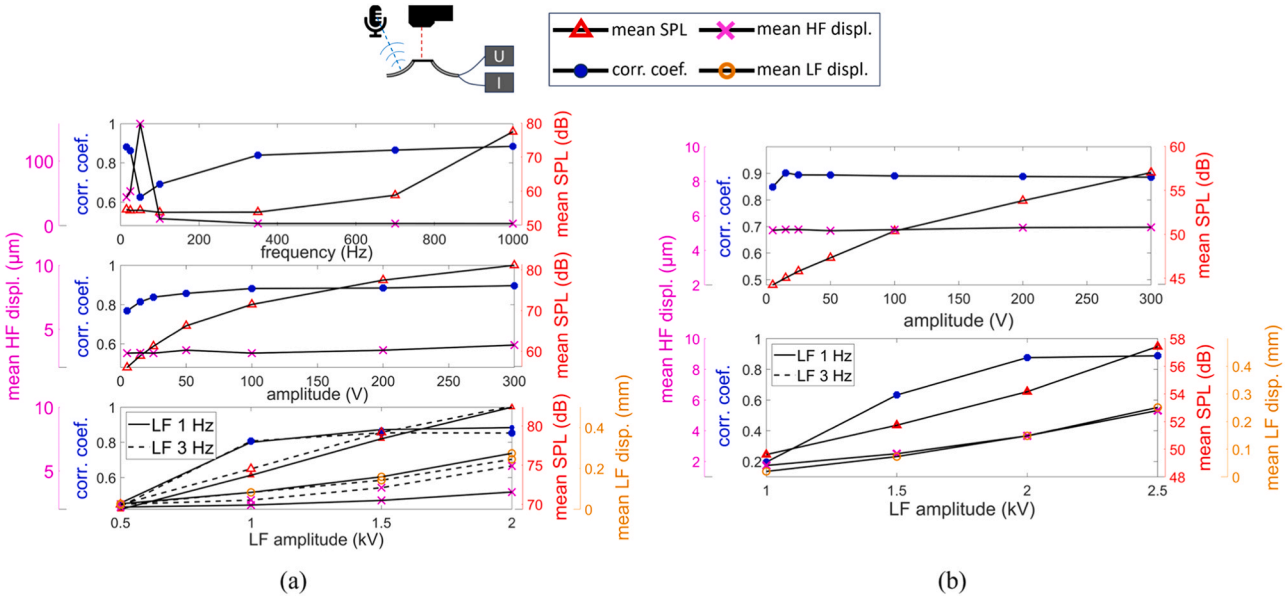

Fig. 10. Characterization of CC (dot-markers) based on self-sensing, SPL (triangular-markers), HF (cross-markers) and LF (circular-markers) mean displacement of the end-effector for different parameter combinations, in the presence of (a) sinusoidal HF signal and (b) polychromatic HF signal.

amplitudes (U_a) involved. HF driving signals $\tilde{u}$ with frequency close to the DEA pumping mode natural frequency strongly contribute to the stroke (see Fig. 10(a) top). In this particular condition, the CC drops down because the contribution of the HF component to the stroke becomes non-negligible, and the frequency of the sensing signal is too low to capture it. The HF signal amplitude and LF signal amplitude have an influence on the CC. As expected, low amplitudes of the LF driving voltage $\bar{u}$ (below 1.5 kV variation) lead to small capacitance variations, that the self-sensing algorithm can only resolve with limited accuracy, leading to minimum CC below 0.5. Using a soundtrack (rather than a monochromatic signal) as $\tilde{u}$ still leads to CCs up to at least 0.8. These results suggest that a frequency of at least 350 Hz and amplitude U_a of at least 50 V is requested for $\tilde{u}$, in order for the self-sensing algorithm to provide CC above 0.8.

5. Proof-of-concept demonstrations

To prove the ability of the self-sensing DEA to concurrently implement 3 working modes (i.e., linear actuation, sound generation, and self-sensing) in practical scenarios, in this section we present results on measurements performed on a set of structured case study demonstrations. These case studies are meant to provide a practical demonstration of the real-time multi-mode self-sensing capability of the system in combination with HF and LF actuation. The considered case studies refer to both scenarios in which the COP-DEA performs tasks involving externally induced deformations (e.g. smart buttons and audio-tactile interfaces), and scenarios involving voltage-driven linear actuation (e.g. obstacle detection, voltage-driven output adaptation).

5.1. Experimental setup

The case studies were run on a dedicated setup, using a real-time target computer (Speedgoat Performance target, 4.2 GHz, 4 cores combined with and IO133 16-bit 200 kSPS, acquiring data at a rate of 200 kSPS), where closed-loop control logics were implemented (using a rate of 20 kHz for the real-time control). The structure of the setup is shown in Fig. 11, with a component diagram of the setup and the signals flow.

A 3 channel high voltage amplifier HAR42–4 with 3 HA3B3-S amplifiers by hivolt.de Gmbh & Co.KG with 3000 V maximum voltage and +/-3 mA maximum current was used as the power supply. The high voltage amplifier has in-built voltage and current monitors, used to measure the output voltage and the current through the DEA. The voltage and current monitors of the amplifier were read with the IO module of the target machine. Measured data were used for the self-sensing algorithm, which run in real-time on the target processor, and resulting capacitance measurements were used to set/adjust the driving

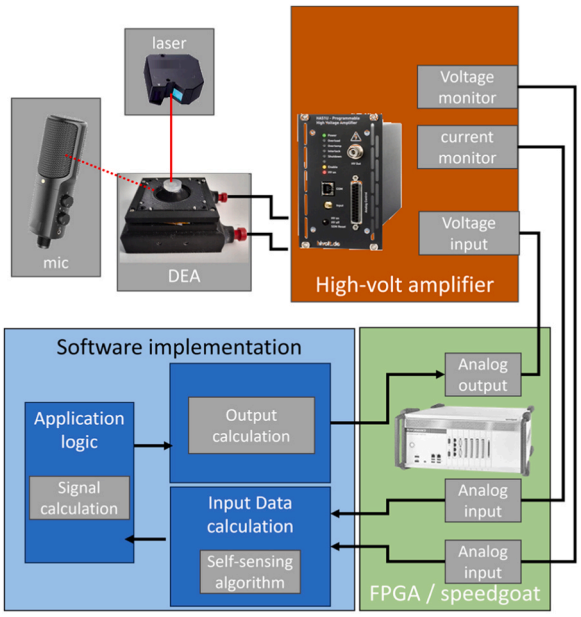

Fig. 11. Test rig setup to measure the performance of the multi-mode DEA in real-time self-sensing application examples.

voltage in a real-time fashion, as per the requirements of the different case studies. Different case studies were implemented by changing the logics coded in the software of the real-time machine, leaving the rest of the setup unchanged. The software implementation made use of Simulink Real-Time™ environment.

Sound measurements were performed using a calibrated microphone NT-USB from RODE placed at 0.25 m far from the specimen. For displacement measurements, an LK-G87 Laser from Keyence was used.

5.2. User-induced movement self-sensing

In the first two examples, the DEA is employed as a user interface (Fig. 3 right), and sensing is used to recognize user-induced deformations that result in a displacement of the DEA end-effector. The deformation is measured via self-sensing, and the output is adjusted depending on either the intensity of touch or the number of consecutive detected touches. Here, the HF driving signal is simultaneously used for audio generation and sensing, and an additional LF signal is possibly used to provide additional tactile feedback.

Since the DEA layers have a capacitance of around 1 nF and the maximum current of the amplifier is 3 mA with maximum voltage of 3 kV, the audio-tactile interface is within the safety limits (20 mA continuous DC current and >100 nF) recommended for DEA interactions with users [32].

5.2.1. Adaptive amplitude adjustment of the HF driving signal

By applying a HF signal with constant amplitude to the prototype, the sound pressure decreases as the user pushes the end-effector down (Fig. 12(a)). This is consistent with previously observed dependences of the DEA sound intensity on the out-of-plane deformation [16]. Leveraging real-time self-sensing, online detection of the out-of-plane deformation of the DEA is possible. Depending on the deformation, the amplitude of the HF signal can be changed to render the sound pressure output of the DEA more uniform. Fig. 12(b) shows the sound pressure output for an amplitude-compensated signal with 1 kHz HF frequency and an amplitude range from $U_{a0} = 100$ V to $U_{a1} = 250$ V (whereas 200 V amplitude was used in the case with constant amplitude). The output amplitude for the compensation is calculated by linear interpolation using the maxima and minima of the capacitance $(C_0; C_1)$ and amplitude $(U_{a0}; U_{a1}) : U_a = U_{a0} + \frac{U_{a1}-U_{a0}}{C_1-C_0}.(C-C_0) = U_{a0} + \frac{\Delta U_a}{\Delta C_0}\Delta C$, with $C_0 > C_1$. The sound pressure is recognizably smoother as compared to Fig. 12(a), showing the potential of self-sensing for equalization of the sound output.

With the simple control logics used in here, which make use of a static mapping of the HF signal amplitude as a function of the capacitance, we could not achieve a completely smooth sound output: significant fluctuations in intensity were still present during fast changes in deformation. A possible way to improve this result is by combining the proposed closed-loop self-sensing-based approach with a filter (based, e.g., on a dynamic model) accounting for the dynamic evolution of the system (rather than just relying on instantaneous capacitance measurements), to adaptively select the HF signal amplitude [33]. Comparison of Fig. 12(a) and (b) shows that the peak sound pressure is lower in the test with compensation (compare video S1, Supporting Information). Reaching a constant pressure output equal to the maxim pressure in Fig. 12(a) (~0.2 Pa) would indeed require voltages that would lead to electric fields higher than the dielectric strength of the material (80–90 V/μm).

5.2.2. Adaptive tactile and acoustic feedback adjustment

In audio-tactile interfaces, self-sensing can be used to change the feedback provided to the user. Adjustments can be done to both the LF (tactile) and the HF (audio) signal simultaneously. In Fig. 13(a), a HF signal is applied to the electrodes with the dual purpose of producing an acoustic output and performing self-sensing, and its pitch is slowly adjusted based on the user's touch intensity. Similar to previously described amplitude adaptation tests, we continuously update the frequency as a function of the measured capacitance. Depending on the implemented logics, the frequency can be increased with the DEA downward deformation (top and middle plots in Fig. 13(a) and video S1,

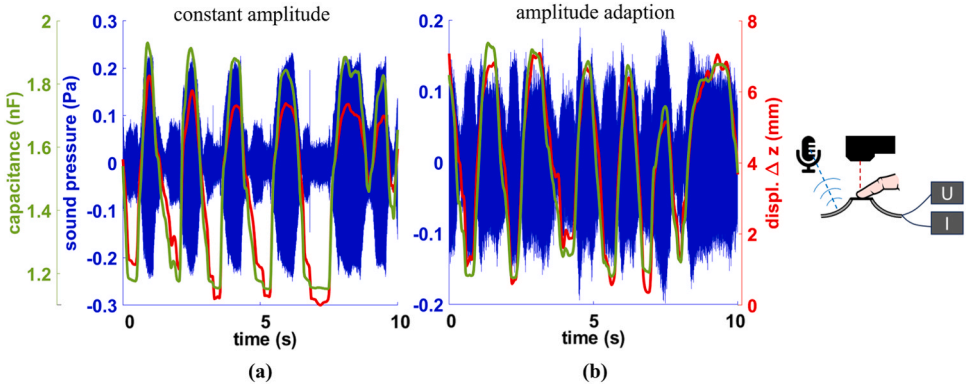

Fig. 12. User induced deformation and corresponding closed-loop amplitude adaption of the HF signal via self-sensing through the HF driving signal applied to the DE.

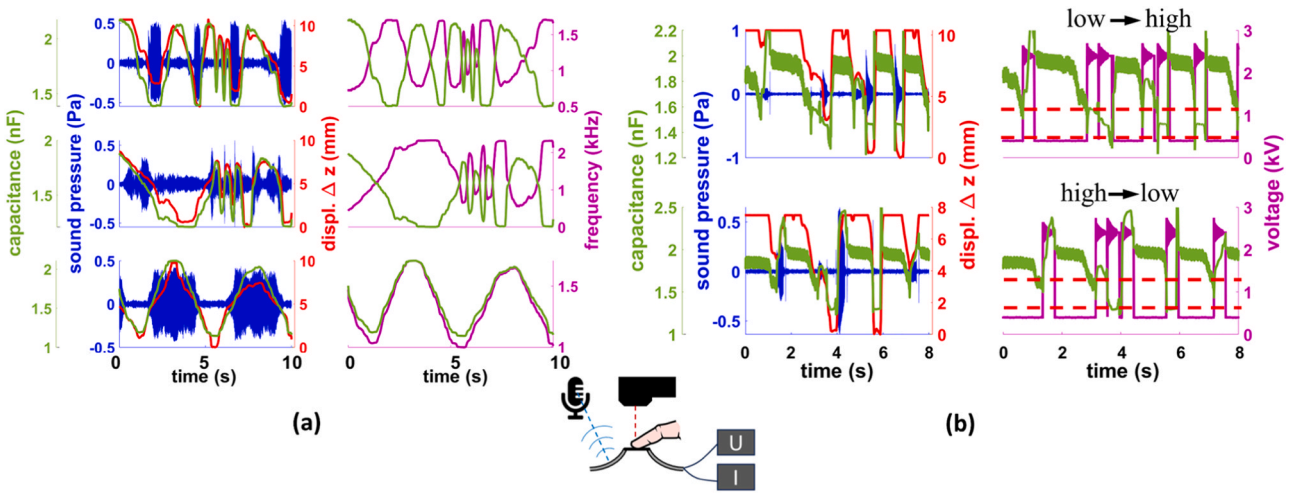

Fig. 13. User-induced deformation and corresponding (a) frequency adaption of the HF signal via self-sensing through the HF signal applied to the DE; (b) haptic and acoustic feedback adaptation via self-sensing through a combination of MF probing signal and HF actuation signal.

Supporting Information) or increased (bottom plot in Fig. 13(a) and video S1, Supporting Information). Since the intensity of the DEA acoustic output varies with the frequency and the amount of deformation, the amplitude of the HF signal might be additionally varied (as in the previous section) to keep the SPL constant.

In a second test (Fig. 13(b) and video S1, Supporting Information), the DEA is used to produce on-demand audio-tactile stimuli that are function of the sensed deformation. In this case, a MF signal (350 Hz) is used for sensing, which generates no feedback until a touch is detected. A set of thresholds values for the capacitance (corresponding to different intensity levels of the touch) are defined (dashed lines in Fig. 13(b)). If the self-sensing algorithm finds that a certain threshold is surpassed, a specific audio-tactile feedback is provided. In Fig. 13(b), two examples of threshold-based feedback are shown. In these tests, two thresholds are implemented: upon reaching the first threshold, a haptic click stimulus (LF signal) with an overlayed acoustic clicking signal (HF signal) is applied, and by reaching the second theshold another feedback with the same tactile stimulus but different acoustic frequency is applied. In the first example in Fig. 13(b) (top plot) a low pitched sound (800 Hz) is produced upon reaching the first threshold, whereas the pitch of the sound is increased to 1800 Hz when the second threshold is reached, whereas the logic is swapped in the second example (from 1500 Hz to 1000 Hz - Fig. 13(b) bottom). While the feedback signal is applied, the self-sensing algorithm still works (relying on currents associated to the HF signal), making it possible to detect whether the user is reaching the second threshold before or after the execution of the first feedback signal is completed. In case the second threshold is surpassed, the execution of the first stimulus is halted, and the second feedback routine, with different HF signal shape, is immediately started. The violet waveforms for the right plots in Fig. 13(b) show the supplied feedback voltage signals which are a LF square wave (resulting in a tactile stimulation) and a superposed sinusoidal HF signal with exponentially decreasing amplitude (resulting in a clicking sound). Both stimuli fall within clearly perceivable tactile/acoustic ranges for users, as demonstrated by previous user tests [17].

A further example of user interaction, which shows the sensing capability also in the presence of arbitrary multi-harmonic HF signals, is shown in the supporting video S4. In that example, the audio output of the DEA (a soundtrack) is changed upon reaching different thresholds for the DE displacement, which is detected via self-sensing based on current measurements associated to the soundtracks reproduction.

5.3. Voltage-induced movement self-sensing

We consider two scenarios involving self-sensing of voltage-induced end effector movements. In the first example, the amplitude of the HF driving signal is varied as a function of the end-effector position, whereas in the second one the impact of the moving end-effector with an obstacle is detected, and an acoustic feedback is produced in response. In both cases, a LF driving signal is superimposed to an HF or MF signal, used for self-sensing. In these examples, the voltage-induced movement of the considered DEA is relatively small (<0.5 mm), because the system (DEA + biasing element) was specifically designed for haptic feedback applications. Nevertheless, the small stroke can still be reliably measured by the self-sensing algorithm and used in a closed-loop setting.

5.3.1. Amplitude adaptation based on self-sensing

As already seen in Section 4, the sound pressure varies strongly with LF displacements of the end-effector. Self-sensing can be used to make the sound intensity steadier by adjusting the HF driving signal amplitude as a function of the deformation.

Fig. 14 shows the end effector displacement, sound pressure time-series, and capacitance (measured via self-sensing) for a sinusoidal driving voltage with HF component at 1 kHz and 250 V maximum amplitude, and LF component with 5 Hz frequency and 750 V amplitude with bias voltage of 2 kV. In Fig. 14(a), the HF component of the driving voltage has constant amplitude of 200 V, which results in a highly variable sound intensity (the sound pressure is maximum when the LF component of the driving voltage, and, hence, the out-of-plane stroke, are maximum). In Fig. 14(b), the HF signal amplitude is continuously varied in a closed-loop fashion, as a function of the measured capacitance, by monotonically decreasing the amplitude with the capacitance either in a linear $\left(U_a = U_{a0} + \frac{\Delta U_a}{\Delta C_0}\Delta C\right)$ or quadratic $\left(U_a = \sqrt{{U_{a0}}^2 + \frac{U_{a1}^2 - U_{a0}^2}{\Delta C_0}\Delta C}\right)$ fashion.

In Fig. 14(c), in contrast, the HF signal amplitude is adjusted as a function of the instantaneous value of the LF driving voltage component (in an open loop fashion), namely, monotonically decreasing the amplitude with increasing values of $\overline{u}(t)$, as previously done in [16]. In both cases, linear and quadratic adaptations of the HF signal amplitude on the capacitance/LF voltage are used (the quadratic dependence being motivated by the quadratic dependence of Maxwell stresses on the voltage). Both compensation methods (self-sensing based closed-loop, and input-based open-loop) lead smoother pressure output trends as compared to the constant amplitude reference scenario (see video S2,

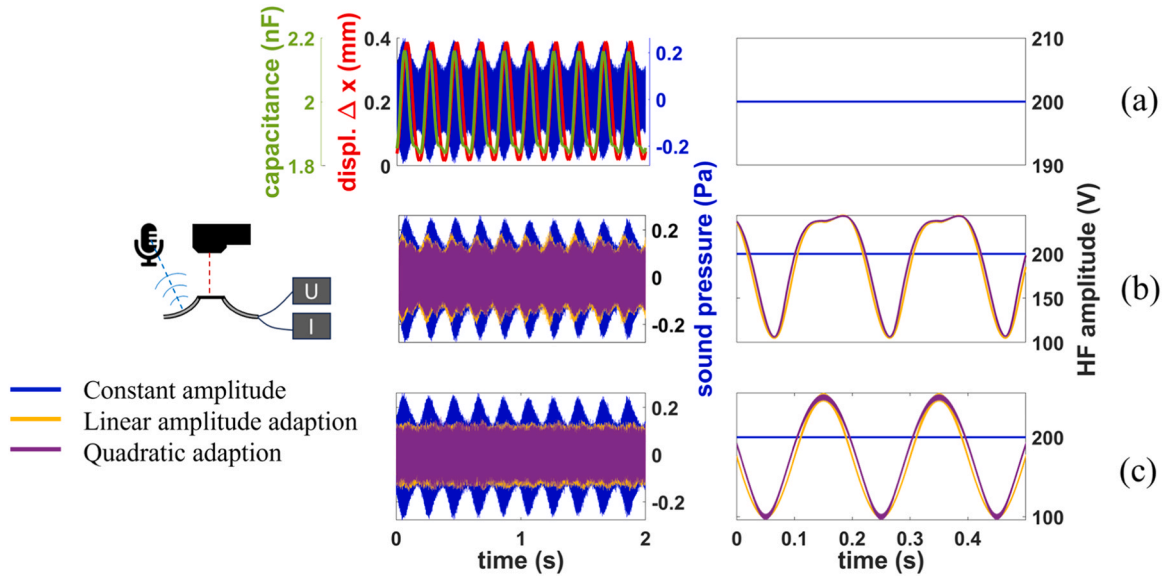

Fig. 14. Adaptation of the HF signal amplitude as a function of voltage-induced deformations. (a) Trends of the end effector displacement, estimated capacitance, and sound pressure time-series (left) in a reference scenario in which the DEA is driven by a constant amplitude HF voltage (right) superposed to a LF driving voltage. (b) Sound pressure obtained by varying the HF signal amplitude as a function of the measured capacitance (self-sensing). (c) Sound pressure obtained by varying the HF signal amplitude as a function of the LF driving signal amplitude (open-loop).

Supporting Information). Quadratic compensations lead to slightly smoother trends as compared to linear adaptation, though their difference is modest, given the small displacements to which the DEA is subject. In these tests, the voltage-based compensation (Fig. 14(c)) is found to provide a smoother sound pressure output than the capacitance-based compensation. This can be explained by the dependence of the sound intensity on the DE membrane tensile stresses, which are influenced by the bias voltage (the higher the bias voltage, the lower the stress on the DE and, hence, its stiffness against structural vibrations). In the conditions of the presented tests, voltage-induced changes in stress have greater influence than the DEA out-of-plane stroke on the sound pressure output, making the open-loop compensation more effective than the simple capacitance-based compensation presented here.

In practice, a better rejection of beat distortions than that achieved in here might be obtained by resorting to more complex compensation approaches, which combine open-loop information on the input voltage with real-time measurements of the capacitance, possibly leveraging dynamic models of the DEA acoustic dynamics. It is also worth remarking that in applications (especially user interaction) the state of the DEA can change because of external factors (impacts, impressed deformations), and such state changes can only be detected through a deformation-based sensing, which necessarily demands for closed-loop logics.

5.3.2. Obstacle detection based on self-sensing

We used self-sensing to provide the DEA device with the ability to detect impact with an obstacle, and respond with a sound feedback. In situations in which the DEA encounters an obstacle during the execution of a stroke, or is subject to loads that are higher than its blocking force, the end effector position will stay constant in spite of input voltage variations. In practice, impact events can be caused by an obstacle located on the DEA trajectory, or a touch by a user. In these situations, the actuator can still generate sound leveraging high-frequency structural modes.

We implemented self-sensing-based obstacle detection by experimentally mapping the static voltage-induced free displacement response of the DEA. We compared such a map with the actual capacitance measurements obtained via self-sensing during LF actuation. We were thus able to identify obstacle impact events by evaluating the difference between expected capacitance and measured capacitance at a given voltage, and verifying whether such difference was above a critical threshold.

We performed two tests (Fig. 15): a first test in which the DEA concurrently produces linear actuation and sound (top row), and a test in which the DEA initially produces silent linear actuation (bottom row). In both tests, the LF component of the driving voltage initially had low amplitude, which was then increased causing the DEA to hit a fixed rigid obstacle located on the end-effector's trajectory. Obstacle detection was performed via self-sensing, respectively using current measurements associated to the HF driving signal (top) or a MF probing signal (bottom). The normalized error between expected capacitance and measured capacitance for the two tests is shown (purple line) on the right plots. During impact events, the error increases over a predefined threshold, leading to the identification of an impact event.

Upon impacts detection, acoustic feedback was produced, by varying the frequency of the (or introducing a) HF driving voltage component (see video S3, Supporting Information).

6. Conclusion

We presented a concept of multi-function dielectric elastomer actuator (DEA) with self-sensing capability. In addition to a previously presented multi-mode actuation principle [16,17], which enables concurrent execution of low frequency (LF) linear actuation and high frequency (HF) sound generation through a DEA membrane driven by a polychromatic input, here we investigate self-sensing approaches that allow detecting LF capacitance variations of the DEA via measurements of currents associated to the HF components of the excitation voltage.

The self-sensing algorithm used in this work relies on an RC model representation of the DEA and a least square regression [21]. Whereas this approach has been applied in the past using dedicated probing voltage signals, superposed to the main driving voltage to obtain readable current measurements, here we prove that the algorithm can be directly run using current measurements associated to the HF component of the driving voltage, even in cases in which such a component is highly multichromatic (e.g., a soundtrack).

We show that, leveraging different regions of the DEA frequency

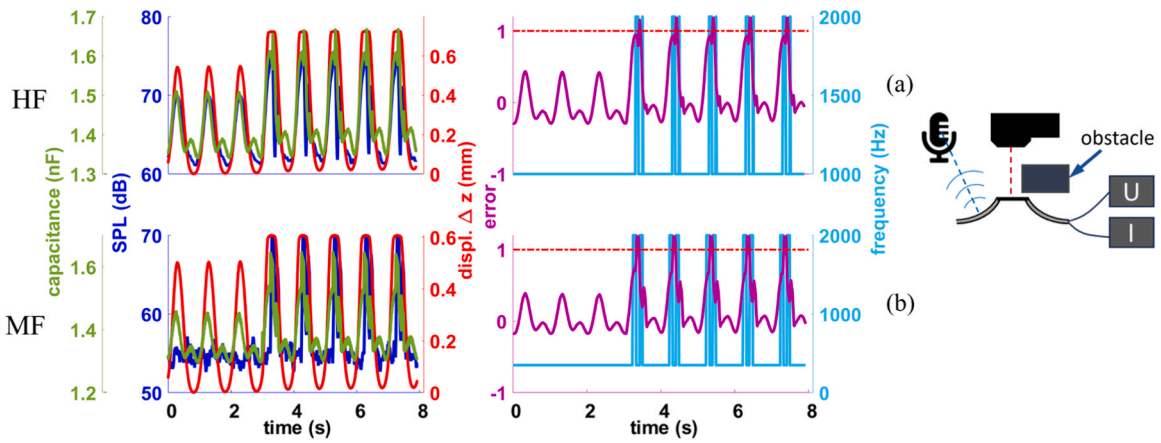

Fig. 15. Obstacle impact detection performed by comparing the expected capacitance and the actual measured capacitance. Top row: the DEA is driven with a HF+LF voltage signal, it produces a linear stroke and sound during the entire test, with the pitch of the sound output changing upon obstacle impact. Bottom row: the DEA is driven with a MF+LF voltage signal, it only produces linear actuation during the first part of the test and generates sound after impact with the obstacle.

response, self-sensing can be performed either in combination with sound generation (exploiting the acoustic driving signal) or alone, while no acoustic output is produced (by using a sensing signal whose frequency is purposedly located outside of both the passbands of the LF pumping motion and the HF structural modes)

We built a 30 mm diameter DEA prototype with multi-layer structure and characterized its ability to accomplish 3 tasks (i.e., LF actuation, sound generation, sensing) at the same time, leveraging different vibration modes of the DEA. We considered different working scenarios for the DEA, in which LF pumping deformations are either driven by an external load (e.g., a push action on the DEA end effector), or a LF driving voltage, and superposed to HF monochromatic or polychromatic acoustic signals. A parameter study for the different cases is presented to validate the correlation of self-sensed capacitance measurements and the DEA deformation. To prove the real-time capability of the proposed self-sensing strategy, application examples are then presented, in which capacitance measurements are used to control and regulate the DEA output in closed-loop. Reference is first made to applications of the DEA as user interface (smart button), in which the amplitude or frequency of the HF voltage excitation is changed as a function of user-induced deformations (e.g., the amount of deformation impressed by a user onto the DEA). Furthermore, in cases in which the DEA concurrently works as a loudspeaker and a linear actuator driven by a single input voltage signal, we investigate the possibility of adaptively adjusting the intensity of the sound pressure output as a function of the stroke, or detect blocking conditions (e.g., impact with an obstacle) and respond with an acoustic warning signal.

The simple case studies presented here show the potential for multi-mode control of DEAs, which might find applications in fields such as wearable sensor-actuator systems, collocated audio-tactile sensing elements or interfaces, and multi-mode actuators that can give feedback depending on their own state (e.g. blocking, overload, or contact with objects).

Future developments will be devoted to improve the correlation between measured capacitance and actual displacement for HF polychromatic input voltages, or increase the sound quality of the interface combining self-sensing and model-based filtering approaches.

CRediT authorship contribution statement

Sebastian Gratz-Kelly: Writing – original draft, Visualization, Validation, Software, Methodology, Investigation, Data curation. **Tim Felix Krüger:** Investigation, Data curation. **Stefan Seelecke:** Writing – review & editing, Supervision, Resources, Project administration. **Gianluca Rizzello:** Writing – review & editing, Methodology, Formal analysis, Data curation. **Giacomo Moretti:** Writing – review & editing, Supervision, Project administration, Methodology, Investigation, Funding acquisition, Conceptualization.

Declaration of Competing Interest

The authors declare the following financial interests/personal relationships which may be considered as potential competing interests: Giacomo Moretti reports financial support was provided by European Commission. If there are other authors, they declare that they have no known competing financial interests or personal relationships that could have appeared to influence the work reported in this paper.

Data Availability

Data will be made available on request.

Acknowledgements

This research received support from the European Union 's Horizon 2020 research and innovation programme under the Marie Skłodowska-Curie grant agreement No 893674 (DEtune), and from the Italian Ministry of Education, University and Research (MUR) under the Program "Departments of Excellence 2023-27" (L.232/2016), awarded to the Department of Industrial Engineering of the University of Trento, Italy.

Appendix A. Supporting information

Supplementary material related to this article can be found online at doi:10.1016/j.sna.2024.115332.

References

[1] R.D. Kornbluh, et al., Electroelastomers: applications of dielectric elastomer transducers for actuation, generation, and smart structures, Smart Struct. Mater. 2002: Ind. Commer. Appl. Smart Struct. Technol. vol. 4698 (2002) 254–270, https://doi.org/10.1117/12.475072.

[2] R.E. Pelrine, R.D. Kornbluh, J.P. Joseph, Electrostriction of polymer dielectrics with compliant electrodes as a means of actuation, Sens Actuators A Phys. vol. 64 (1) (1998) 77–85, https://doi.org/10.1016/S0924-4247(97)01657-9.

[3] F. Carpi, D. De Rossi, R. Kornbluh, R. Pelrine, P. Sommer-Larsen, Dielectric Elastomers as Electromechanical Transducers: Fundamentals, Materials, Devices, Models and Applications of an Emerging Electroactive Polymer Technology. Dielectric Elastomers as Electromechanical Transducers, Elsevier, 2008, p. 329, https://doi.org/10.1016/B978-0-08-047488-5.X0001-9.

[4] R. Pelrine, R. Kornbluh, Q. Pei, J. Joseph, High-speed electrically actuated elastomers with strain greater than 100 %, Science vol. 287 (5454) (2000) 836–839, https://doi.org/10.1126/SCIENCE.287.5454.836.

[5] Y. Chen, L. Agostini, G. Moretti, M. Fontana, R. Vertechy, Dielectric elastomer materials for large-strain actuation and energy harvesting: a comparison between styrenic rubber, natural rubber and acrylic elastomer, Smart Mater. Struct. vol. 28 (11) (2019) 114001, https://doi.org/10.1088/1361-665X/AB3B32.
[6] A. Khurana, A.K. Sharma, · M.M. Joglekar, Nonlinear oscillations of electrically driven aniso-visco-hyperelastic dielectric elastomer minimum energy structures, vol. 104, pp. 1991–2013, 2021, doi: ⟨10.1007/s11071-021-06392-5⟩.
[7] A.K. Sharma, M. Kosta, G. Shmuel, O. Amir, Gradient-based topology optimization of soft dielectrics as tunable phononic crystals, Compos Struct. vol. 280 (Jan. 2022) 114846, https://doi.org/10.1016/J.COMPSTRUCT.2021.114846.
[8] E. Garnell, O. Doaré, C. Rouby, O. Doar, Coupled vibro-acoustic modeling of a dielectric elastomer loudspeaker, J. Acoust. Soc. Am. vol. 147 (3) (2020) 1812–1821, https://doi.org/10.1121/10.0000930.
[9] T. Sugimoto, et al., A lightweight push-pull acoustic transducer composed of a pair of dielectric elastomer films, J. Acoust. Soc. Am. vol. 134 (5) (2013) EL432–EL437, https://doi.org/10.1121/1.4824631.
[10] H. Zhao, et al., A wearable soft haptic communicator based on dielectric elastomer actuators, Soft Robot vol. 7 (4) (Aug. 2020) 451–461, https://doi.org/10.1089/SORO.2019.0113.
[11] A. Marette, A. Poulin, N. Besse, S. Rosset, D. Briand, H. Shea, Flexible zinc–tin oxide thin film transistors operating at 1 kV for integrated switching of dielectric elastomer actuators arrays, Adv. Mater. vol. 29 (30) (2017), https://doi.org/10.1002/ADMA.201700880.
[12] D.Y. Lee, et al., A wearable textile-embedded dielectric elastomer actuator haptic display, Soft Robot vol. 9 (6) (2022) 1186–1197, https://doi.org/10.1089/SORO.2021.0098.
[13] G. Frediani, D. Mazzei, D.E. De Rossi, F. Carpi, Wearable wireless tactile display for virtual interactions with soft bodies, Front Bioeng. Biotechnol. vol. 2 (2014) 31, https://doi.org/10.3389/FBIOE.2014.00031/BIBTEX.
[14] X. Ji, et al., Untethered feel-through haptics using 18-μm thick dielectric elastomer actuators, Adv. Funct. Mater. vol. 31 (39) (2021) 2006639, https://doi.org/10.1002/ADFM.202006639.
[15] H. Phung, et al., Tactile display with rigid coupling based on soft actuator, Meccanica vol. 50 (11) (2015) 2825–2837, https://doi.org/10.1007/S11012-015-0270-5/FIGURES/19.
[16] S. Gratz-Kelly, G. Rizzello, M. Fontana, S. Seelecke, G. Moretti, A multi-mode, multi-frequency dielectric elastomer actuator, Adv. Funct. Mater. vol. 32 (34) (2022), https://doi.org/10.1002/adfm.202201889.
[17] S. Gratz-Kelly, T.F. Krüger, G. Rizzello, S. Seelecke, G. Moretti, An audio-tactile interface based on dielectric elastomer actuators, Smart Mater. Struct. vol. 32 (3) (2023) 034005, https://doi.org/10.1088/1361-665X/ACB6DA.
[18] G. Rizzello, D. Naso, A. York, S. Seelecke, Closed loop control of dielectric elastomer actuators based on self-sensing displacement feedback, Smart Mater. Struct. vol. 25 (3) (2016) 035034, https://doi.org/10.1088/0964-1726/25/3/035034.
[19] T.A. Gisby, B.M. Obrien, I.A. Anderson, Self sensing feedback for dielectric elastomer actuators, Appl. Phys. Lett. vol. 102 (19) (2013), https://doi.org/10.1063/1.4805352.
[20] T. Hoffstadt, J. Maas, Self-sensing control for soft-material actuators based on dielectric elastomers, Front Robot AI vol. 6 (2019) 496444, https://doi.org/10.3389/FROBT.2019.00133/BIBTEX.
[21] G. Rizzello, D. Naso, A. York, S. Seelecke, A self-sensing approach for dielectric elastomer actuators based on online estimation algorithms, IEEE/ASME Trans. Mechatron. vol. 22 (2) (2017) 728–738, https://doi.org/10.1109/TMECH.2016.2638638.
[22] G. Rizzello, F. Fugaro, D. Naso, S. Seelecke, Simultaneous self-sensing of displacement and force for soft dielectric elastomer actuators, IEEE Robot Autom. Lett. vol. 3 (2) (2018) 1230–1236, https://doi.org/10.1109/LRA.2018.2795016.
[23] K. Jung, J. Kim, H.R. Choi, A self-sensing dielectric elastomer actuator, Sens. Actuators A vol. 143 (2008) 343–351, https://doi.org/10.1016/j.sna.2007.10.076.
[24] S. Gratz-Kelly, T. Krüger, S.Seelecke, G. Rizzello, and G. Moretti, A self-sensing approach for multi-mode dielectric elastomer actuator-loudspeaker devices, In Electroactive Polymer Actuators and Devices (EAPAD) XXV (Vol. 12482, pp. 21-31). SPIE.
[25] C. Cao, X. Gao, A.T. Conn, A magnetically coupled dielectric elastomer pump for soft robotics, Adv. Mater. Technol. vol. 4 (8) (2019), https://doi.org/10.1002/ADMT.201900128.
[26] G. Berselli, R. Vertechy, G. Vassura, V. Parenti-Castelli, Optimal synthesis of conically shaped dielectric elastomer linear actuators: design methodology and experimental validation, IEEE/ASME Trans. Mechatron. vol. 16 (1) (2011) 67–79, https://doi.org/10.1109/TMECH.2010.2090664.
[27] M. Jabareen, M. Eisenberger, Free vibrations of non-homogeneous circular and annular membranes, J. Sound Vib. (3) (2001) 409–429, https://doi.org/10.1006/jsvi.2000.3249.
[28] B. Fasolt, M. Hodgins, S. Seelecke, Characterization of screen-printed electrodes for dielectric elastomer (DE) membranes: influence of screen dimensions and electrode thickness on actuator performance, in: in Electroactive Polymer Actuators and Devices (EAPAD), Vol. 9798, SPIE, 2016, pp. 662–672, https://doi.org/10.1117/12.2222095.
[29] B. Fasolt, M. Hodgins, G. Rizzello, S. Seelecke, Effect of screen printing parameters on sensor and actuator performance of dielectric elastomer (DE) membranes, Sens Actuators A Phys. vol. 265 (2017) 10–19, https://doi.org/10.1016/J.SNA.2017.08.028.
[30] Project Nayuki web site, ⟨https://www.nayuki.io/page/transcription-of-pokemon-game-boy-music⟩, (Accessed: October 2023).
[31] J. Cohen, Statistical Power Analysis for the Behavioral Sciences, Routledge, 2013.
[32] S. Pourazadi, A. Shagerdmootaab, H. Chan, M. Moallem, C. Menon, On the electrical safety of dielectric elastomer actuators in proximity to the human body, Smart Mater. Struct. vol. 26 (11) (2017), https://doi.org/10.1088/1361-665X/AA89B1.
[33] T. Hoffstadt, J. Maas, Model-based self-sensing algorithm for dielectric elastomer transducers based on an extended Kalman filter, Mechatronics vol. 50 (2018) 248–258, https://doi.org/10.1016/J.MECHATRONICS.2017.09.013.

Sebastian Gratz-Kelly is a Ph D. student at the intelligent Material Systems Lab of the Saarland university and Group leader for Smart Textiles. He received his B.Sc. in 2014 and M. Sc. in 2017 from Saarland university, department of systems engineering. His research topics are sensor and actuator systems based on dielectric elastomers, smart textiles and textile integration, as well as user interaction.

Tim Krüger is a Bachelor student at Saarland University in the field of Systems Engineering. He works as a student assistant for the Smart Textiles group, at the Intelligent Material Systems Lab. His tasks include design and maintenance of testbenches and demonstrators for dielectric elastomer sensors and actuators, experimental data acquisition and management.

Stefan Seelecke received his Ph.D. degree in Engineering Science from Technical University Berlin, Berlin, Germany in 1995. After his habilitation in 1999, he joined the Department of Mechanical and Aerospace Engineering at North Carolina State University, Raleigh, USA, in 2001. He is currently a Full Professor of Systems Engineering and Materials Science & Engineering at Saarland University, Saarbrücken, Germany, where he directs the Intelligent Material Systems Lab. His research interests include the development of smart materials-based actuator and sensor systems, in particular (magnetic) shape memory alloys, piezoelectrics and electroactive polymers.

Gianluca Rizzello was born in Taranto, Italy, in 1987. He received the master's (Hons.) degree in control engineering from the Polytechnic University of Bari, Bari, Italy, in 2012. He received his Ph.D. in Information and Communication Technologies from Scuola Interpolitecnica di Dottorato, a joint program between Polytechnic Universities of Torino, Bari, and Milano, Italy, in 2016. After his doctoral studies, he joined the Saarland University, Saarbrücken, Germany, first with the role of a postdoc researcher and Group Leader Smart Material Modeling and Control (2016–2019), and subsequently as Assistant Professor in Adaptive Polymer Systems (2020 - present). His research interests involve modeling, control, and self-sensing of innovative mechatronic and robotic systems based on unconventional drive technologies, such as smart materials.

Giacomo Moretti holds a MSc degree in Energy Engineering (University of Pisa - 2013) and a PhD in Mechanical Engineering (Scuola Sant'Anna - 2017). He has been a visiting scholar at the University of Edinburgh, UK (2016), and a research fellow at Scuola Sant'Anna, Italy (2017–2020) and Saarland University, Germany (2020–2022), which he joined with a Marie-Curie fellowship. Since 2022, he has been assistant professor (tenure track) at the University of Trento (IT). His research covers the fields of multifunctional transducers and energy harvesting. His main contributions regard the development and validation of ocean wave energy harvesting concepts based on electroactive-polymers; smart-material-based electrostatic loudspeakers and user interfaces; thermo- and electro-active robotic artificial muscles.